PHOTONICS Research

Towards optimum Franson interference recurrence in mode-locked singly-filtered biphoton frequency combs

Kai-Chi Chang,[1,†,*] Xiang Cheng,[1,2,†] Murat Can Sarihan,[1] and Chee Wei Wong[1,3]

[1]Fang Lu Mesoscopic Optics and Quantum Electronics Laboratory, Department of Electrical and Computer Engineering, University of California, Los Angeles, California 90095, USA
[2]e-mail: chengxiang@ucla.edu
[3]e-mail: cheewei.wong@ucla.edu
[†]These authors contributed equally to this work.
[*]Corresponding author: uclakcchang@g.ucla.edu

Received 14 December 2022; revised 21 March 2023; accepted 19 April 2023; posted 21 April 2023 (Doc. ID 483570); published 16 June 2023

Mode-locked biphoton frequency combs exhibit multiple discrete comblike temporal correlations from the Fourier transform of its phase-coherent frequency spectrum. Both temporal correlation and Franson interferometry are valuable tools for analyzing the joint properties of biphoton frequency combs, and the latter has proven to be essential for testing the fundamental quantum nature, the time-energy entanglement distribution, and the large-alphabet quantum key distributions. However, the Franson recurrence interference visibility in biphoton frequency combs unavoidably experiences a falloff that deteriorates the quality of time-energy entanglement and channel capacity for longer cavity round trips. In this paper, we provide a new method to address this problem towards optimum Franson interference recurrence. We first observe mode-locked temporal oscillations in a 5.03 GHz free-spectral range singly filtered biphoton frequency comb using only commercial detectors. Then, we observe similar falloff trend of time-energy entanglement in 15.15 GHz and 5.03 GHz free-spectral range singly filtered biphoton frequency combs, whereas, the optimum central time-bin accidental-subtracted visibility over 97% for both cavities. Here, we find that by increasing the cavity finesse F, we can enhance the detection probability in temporal correlations and towards optimum Franson interference recurrence in our singly filtered biphoton frequency combs. For the first time, via a higher cavity finesse F of 45.92 with a 15.11 GHz free-spectral range singly filtered biphoton frequency comb, we present an experimental ≈3.13-fold improvement of the Franson visibility compared to the Franson visibility with a cavity finesse F of 11.14 at the sixth time bin. Near optimum Franson interference recurrence and a time-bin Schmidt number near 16 effective modes in similar free-spectral range cavity are predicted with a finesse F of 200. Our configuration is versatile and robust against changes in cavity parameters that can be designed for various quantum applications, such as high-dimensional time-energy entanglement distributions, high-dimensional quantum key distributions, and wavelength-multiplexed quantum networks.

https://doi.org/10.1364/PRJ.483570

1. INTRODUCTION

Mode-locked biphoton states, exhibiting unique discrete spectral and temporal multimode behavior within a single spatial mode profile, can be generated by spontaneous parametric down-conversion (SPDC) photons via cavity filtering [1–5], cavity enhancement [6–16], and by spontaneous four-wave mixing in integrated microring resonators [17–21]. The mode-locked behavior in a biphoton frequency comb (BFC) manifests itself as interesting comblike temporal correlations via Hanbury–Brown–Twiss-type interferometry [7–10,14,16,22], which can be naturally exploited by direct joint temporal intensity (JTI) measurements to verify high-dimensional frequency-bin entanglement with complementary joint spectral intensity (JSI) measurements [23]. Such oscillations in the temporal domain can also be used in chip-scale optical quantum information processing [24–27], in time-bin-based quantum communication protocols [28–32], and in quantum networks based on time-resolved correlation measurements [33,34], including multiboson correlation sampling schemes [35,36].

Time-energy entanglement, first formulated by Franson using a pair of unbalanced Mach–Zehnder interferometers (MZIs) [37], has proven to be quintessential from fundamental

and practical perspectives in the quantum optics community. For example, the Franson interference is important for testing quantum nature in a loophole-free test [38] for high-quality long-distance time-energy entanglement distribution [39–44] and for securing time-bin-based high-dimensional quantum key distribution (QKD) against collective Gaussian attacks [29,45,46]. This distinct mode-locked feature of BFC can be revealed nonlocally via a Franson interferometry, leading to discrete time-energy-entangled Franson interference recurrences, spaced by the round-trip time of the cavity [2–5]. The cavity geometry, the reflectivity of the mirrors, finesse F, and the free spectral range (FSR) of the cavity determine the JSI and the JTI of the generated mode-locked BFC states. Indeed, the cavity serves as a tool to tailor the parameters of the two-photon state via the two-photon mode-locked process, for instance, to probe the time-energy entanglement via Franson interferometry using off-the-shelf telecom compatible filters [2–5] or to match the bandwidth of the SPDC photons to a specific atomic transition line for quantum memory storage [11–13,15,47–52]. Moreover, to the best of our knowledge, in all of the previous demonstrations for cavity-filtered mode-locked BFCs [1–5], the impact of the key figure of merit, the cavity finesse F on both mode-locked temporal correlations, and Franson interference recurrences remain unexplored.

In this paper, we utilize mode-locked singly filtered BFCs based on the cavity-filtered scheme with a Fabry–Perot (FP) cavity that is flexible and robust for experimental implementations. We examine the role of cavity finesse F in the mode-locked signal-idler temporal cross correlations as well as in the time-energy entanglement via Franson interferometry with our experimental demonstrations and theoretical descriptions. First, we observe the mode-locked temporal oscillations of a singly filtered BFC using our second-order cross-correlation function measurements with a cavity FSR of 5.03 GHz and a bandwidth of 457 MHz. Such direct JTI measurements using commercial single-photon detectors signify the existence of spectral phase coherence in the cavity-filtered BFC scheme for the first time. Second, we measure and quantify the falloff trend of the time-energy entanglement in our singly filtered BFCs based on 15.15 GHz and 5.03 GHz cavities via Franson interferometry, spanning up to six time bins with the highest central time-bin accidental-subtracted visibility over 97% for both cavities. Such JSI measurements are consistent and complementary with our JTI measurements. We find out the cavity finesse F plays a central role towards optimum temporal correlations and Franson interference recurrence in our singly filtered mode-locked BFCs by comparing different cavity configurations. For the first time, via a higher cavity finesse F of 45.92 in a 15.11 GHz BFC, we measured a Franson recurrence visibility of 69.86% with an approximately 3.13-fold improvement of Franson visibility compared to the Franson visibility with cavity finesse F of 11.14 at the sixth time bin, approaching the quantum-classical limit of 70.7%. Moreover, for the 16th time bin in the same BFC, there is a potential approximately 24-fold improvement of the Franson visibility for a cavity finesse F of 45.92 compared to the Franson visibility with a cavity finesse F of 11.14. Near-optimum Franson interference recurrence and a time-bin Schmidt number K_T near 16 effective modes in similar FSR fiber cavity are predicted with a cavity finesse F of 200. Our results pave the way for producing high-quality mode-locked temporal correlations for time-resolved correlation-based quantum networks and can be helpful in pushing the limit of the Hilbert space dimensionality in the temporal domain [3], for high-quality long-distance high-dimensional time-energy entanglement distributions [4,53,54] and on-chip optical quantum information processing.

2. RESULTS AND DISCUSSION

A. Experimental Setup

The working principle of our experiment is illustrated in Fig. 1(a). We used singly filtered mode-locked BFC sources where the SPDC source is a fiber-coupled type-II phase-matched periodically poled KTiOPO4 (ppKTP) waveguide of fiber-coupling efficiency of ≈50% per facet, driven by a self-injection-locked continuous-wave laser at 658 nm wavelength [55]. The singly filtered BFCs are generated by sending the signal photon of the orthogonally polarized frequency-degenerate photon pairs at 1316 nm with a 245 GHz FWHM phase-matching bandwidth to three fiber FP cavities with

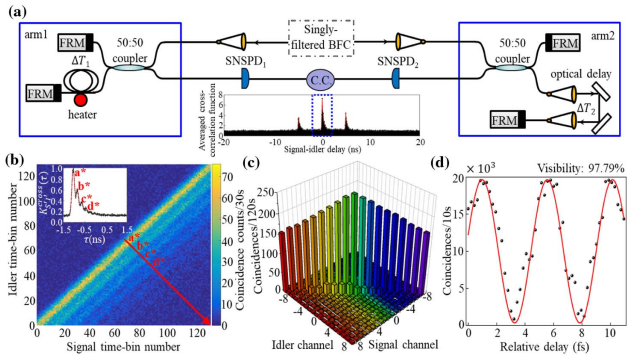

Fig. 1. Measured single-photon cross correlations and time-energy entanglement using a 5.03 GHz FSR singly filtered BFC. (a) Schematic of experimental configuration. FRM, Faraday mirror; C.C., coincidence counts; SNSPD, superconducting nanowire single-photon detector. Inset: the signature of observed Franson interferences, with the single-sided correlation function revealed (see the highlighted region in the blue dashed lines). (b) Measured JTI of a 5.03 GHz FSR singly filtered BFC. The photon coincidence data are recorded between two detectors, and we sift the coincidence data into frames of duration $d \times T_{\text{bin}}$, composed of d time bins of duration T_{bin}. We choose T_{bin} to be 16 ps to enhance the resolution of temporal correlations. This d of 128 shows that there are ∼4 clean cross correlations from a* to d* in our 5.03 GHz singly filtered BFC. The red arrow indicates both the cross sections of measured JTI [also shown in the inset of (b)], and the direction of singly filtered temporal waveform. Inset: measured zoom-in second-order cross-correlation function between signal and idler photons. The periodic structure traces the cavity round-trip time of 198.9 ps. A cavity bandwidth of 457 MHz can be derived by the exponential decay of the envelope. Our result in the inset of (b) is consistent with our results in (b). (c) Example measured JSI of a 5.03 GHz FSR singly filtered BFC. For these measurements, we use a pair of tunable frequency filters to scan from the −9 to +9 frequency bins. (d) The observed quantum time-energy entanglement of a 5.03 GHz FSR singly filtered BFC source and witnessed Franson fringe with an accidental-subtracted visibility of 97.79% for central time bin.

5.03 GHz, 15.11 GHz, and 15.15 GHz FSR, respectively. The idler photon is untouched. The cavity FWHM bandwidths are 0.46 GHz, 0.329 GHz, and 1.36 GHz, respectively. The generated singly filtered mode-locked BFCs state is then directed to a stabilized Franson interferometer for nonlocal interference measurements. After the Franson interferometer, coincidences are recorded with two commercial superconducting nanowire single-photon detectors (SNSPDs, ≈85% detection efficiency and root-mean-square timing jitter ≈55 ps, PhotonSpot, Inc.). We first measure the quantum signature of Franson interference, the three temporally separated correlation peaks as presented in the inset of Fig. 1(a). We observe clear single-sided temporal second-order cross-correlation structures for all Franson correlation peaks. Details of the experimental setup for singly filtered mode-locked BFC sources can be found in Fig. 5 of Appendix A.

Our Franson interferometry is composed of two unbalanced MZIs with the path-length difference measured to be $\Delta T = 4.84$ ns, supporting the probing of time-energy entanglement [37]. We use a thermal heater in the long path of arm1 to sweep and fine-tune the relative phase shift ΔT_1 between the two MZIs to probe the time-energy entanglement of our singly filtered BFCs. In addition, a motorized stage delay in arm2 with ΔT_2 up to 360 ps is used to select different time bins, and temperature controllers with long-term temperature stability of ≈1 mK are implemented to stabilize our Franson interferometry.

B. Model of Mode-Locked Singly Filtered BFCs

Here, we analyze the role of cavity finesse F in the model of mode-locked singly filtered BFC, focusing on temporal second-order cross-correlation function and Franson interference recurrences based on our experimental setup. The mode-locked signal-idler temporal second-order cross-correlation function of singly filtered BFC can be written as [4,8,14]

$$K^{\text{cross}}_{S'I'}(\tau)=\int_{-\infty}^{\infty}\frac{\mathrm{d}\omega i\sqrt{N_S}\,\text{sinc}(\omega t_{\text{coh}}/2)e^{-4\omega^2\ln(2)/\Delta\omega^2}e^{i\omega(\tau-t_{\text{coh}}/2)}}{1+i\frac{1}{\pi F}\sin(\pi\omega/\Delta\Omega)e^{-i\pi\omega/\Delta\Omega}}. \tag{1}$$

Here, $\tau = t_{\text{signal}} - t_{\text{idler}}$; N_S is the source brightness; $t_{\text{coh}} = 3.62$ ps is the coherence time of our SPDC source; and $\Delta\omega/2\pi = 225$ GHz is the FWHM bandwidth of the Gaussian bandpass filter (BPF). The key figure-of-merit cavity finesse F is given by

$$F=\frac{\Delta\Omega}{2\Delta\omega_c}=\frac{\pi}{\Delta\omega_c\Delta T_{\text{cavity}}}=\frac{\pi}{\arcsin\left(\frac{1-\sqrt{1-l_{\text{rt}}}}{2\sqrt[4]{1-l_{\text{rt}}}}\right)}=\frac{\lambda Q}{2L}, \tag{2}$$

where $\Delta\Omega$ is the FSR of the cavity; $\Delta\omega_c$ is the cavity bandwidth; ΔT_{cavity} is cavity round-trip time; l_{rt} is the total round-trip optical losses including scattering losses, clipping losses, absorption and transmission losses; λ is the cavity mode wavelength; Q is the cavity quality factor; and L is the cavity optical length. For a linear planar FP cavity, the cavity finesse F is proportional to cavity quality factor Q.

By using Eqs. (1) and (2), we obtain the Franson interference recurrence envelopes with maximum and minimum coincidence counts as follows:

$$\begin{aligned}C^{\max}_{S'I'}(\tau)=\frac{\eta'_S\eta'_I}{16}\int_0^{T_g}\mathrm{d}\tau[&(|K^{(\text{cross})}_{S'I'}(\tau)|^2)\\&+|K^{(\text{cross})}_{S'I'}(\tau-n\Delta T_{\text{cavity}})|^2\\&+2|K^{(\text{cross})*}_{S'I'}(\tau)K^{(\text{cross})}_{S'I'}(\tau-n\Delta T_{\text{cavity}})|^2],\end{aligned} \tag{3}$$

and

$$\begin{aligned}C^{\min}_{S'I'}(\tau)=\frac{\eta'_S\eta'_I}{16}\int_0^{T_g}\mathrm{d}\tau[&(|K^{(\text{cross})}_{S'I'}(\tau)|^2)\\&+|K^{(\text{cross})}_{S'I'}(\tau-n\Delta T_{\text{cavity}})|^2\\&-2|K^{(\text{cross})*}_{S'I'}(\tau)K^{(\text{cross})}_{S'I'}(\tau-n\Delta T_{\text{cavity}})|^2],\end{aligned} \tag{4}$$

where η'_S, η'_I include all losses encountered in our measurement setup and T_g is the coincidence counting window of 2 ns. Subsequently we can obtain the Franson interference recurrence visibilities at the nth time bin in a singly filtered BFC to be

$$V_n = \exp(-n\pi/F). \tag{5}$$

Equations (1) and (5) allow us to evaluate the impact of cavity finesse F on the signal-idler temporal second-order cross-correlation function and visibilities for the Franson interference recurrence numerically, enabling the comparison with our experimental measurements of singly filtered mode-locked BFCs.

C. Experimental and Theoretical Results

Next, in Fig. 1(b), by using experimental setup in Fig. 5 of Appendix A, we measure the JTI of our 5.03 GHz FSR singly filtered BFC using large-alphabet encoding [29]. We sift the coincidence data into frames of duration $d \times T_{\text{bin}}$, composed of d time bins of duration T_{bin}. We choose T_{bin} to be 16 ps to enhance the resolution of temporal correlations. This d of 128 shows that there are ∼4 clean cross correlations from a^* to d^* in our 5.03 GHz singly filtered BFC. The red arrow indicates both the cross sections of measured JTI [also shown in the inset of Fig. 1(b)], and the decay direction of singly filtered temporal waveform. The inset of Fig. 1(b) shows the corresponding $g^{(2)}$ measurements of the signal-idler temporal second-order cross-correlation function for the same singly filtered BFC. Using a 5.03 GHz FSR fiber cavity and commercial SNSPDs, we observe a clear comblike structure of the temporal correlation, resulting from the mode-locking process of our singly filtered BFC source. The time interval t_{rt} is measured to be ≈200 ps, which matches well with a cavity FSR of 5.03 GHz (≈198.8 ps). Cavity damping rate is extracted to be ≈458.7 MHz from our measurements with the exponential decay of the mode-locked oscillations envelope, and this value closely matches the cavity bandwidth of 457 MHz [8,9]. Our result in the inset of Fig. 1(b) is consistent with our results in Fig. 1(b). This is the first experimental measurement of signal-idler temporal second-order cross-correlation function that probes the JTI in cavity-filtered BFC scheme using only commercial detectors, certifying the existence of phase coherence for our multimode quantum source. Such JTI measurements, when paired with JSI measurements [example JSI measurements for the same singly filtered BFC are shown in Fig. 1(c), where we scan multiple frequency bins within the

phase-matching bandwidth of our biphoton source using a pair of tunable frequency filters], reveal genuine high-dimensional frequency-bin entanglement via providing mutual information of biphoton phase coherence [23].

We next perform Franson interference measurements for the 5.03 GHz FSR singly filtered BFC. Figure 1(d) shows the optimized maximum Franson interference of the central time bin in a 5.03 GHz FSR cavity. For this measurement, we sweep the thermal heater in arm1 to tune the relative phase-shift ΔT_1 between the two MZIs, whereas, fixing the motorized stage position ΔT_2 at the center of the optimum Franson interference. By postselecting coincidence events occurring within a 2 ns wide coincidence time window, while changing the phases of the interferometers (ΔT_1), we obtain a maximum visibility of 97.79% for the 5.03 GHz FSR singly filtered BFC, after accidental coincidence subtraction. The Franson visibility is calculated based on $(C_{\max} - C_{\min})/(C_{\max} + C_{\min})$, where $C_{\max}$ is the maximum interference fringe coincidence counts and $C_{\min}$ is the minimum interference fringe coincidence counts.

Due to the mode-locking process of our singly filtered BFC, the two-photon mode-locked oscillations in the temporal domain will result in discretized time-energy entanglement. Indeed, by using both 5.03 GHz and 15.15 GHz FSR singly filtered BFCs, we measure the Franson interference recurrences over two and six time bins, respectively, as presented in Fig. 2. For a 15.15 GHz FSR singly filtered BFC, we observe the Franson interference fringes visibilities to be 98.97%, 74.32%, 54.37%, 40.56%, 31.50%, and 22.32%, after subtracting the accidental coincidence counts as shown in Figs. 2(a)–2(f) (see Fig. 6 in Appendix B for the measured quantum signatures of Franson interferences for the 15.15 GHz FSR singly filtered BFC). Then, in Fig. 2(g), we compare our experimental results with theoretical modeling. In the insets of Fig. 2(g), we observe Franson interference fringes visibilities to be 97.79% and 72.32%, after accidental coincidence subtraction for the 5.03 GHz FSR singly filtered BFC. The number of measurable time bins is limited by both the FSR of the cavity and the motorized stage position ΔT_2 in arm2 of our Franson interferometer. Besides, we also measure the noninteger cavity round-trip-time Franson interferences for the center time bin in both singly filtered BFCs. This is illustrated in Fig. 7 of Appendix B with an absence of the Franson interference fringes, which confirms the discretization of singly filtered BFCs due to mode-locking process. These JSI measurements are consistent with our JTI measurements in Fig. 1(b) of ≈200 ps cavity round-trip time, confirming the mode-locked phase coherence behavior of our singly filtered BFC.

Interestingly, we find that although these two cavities have different FSRs and cavity bandwidths, they have similar cavity finesse F ($F_{5.03\,\mathrm{GHz}} = 10.93$ and $F_{15.15\,\mathrm{GHz}} = 11.14$), resulting in the close trend of the recurrence visibilities in the Franson interference, illustrated by bidirectional black arrows in Fig. 2(g) between experiment and theory. This indicates that the cavity finesse F plays a key role in determining the quality of time-energy entanglement over multiple time bins. By increasing this figure of merit, the falloff of Franson interference recurrence visibilities over multiple cavity round-trip times can be improved.

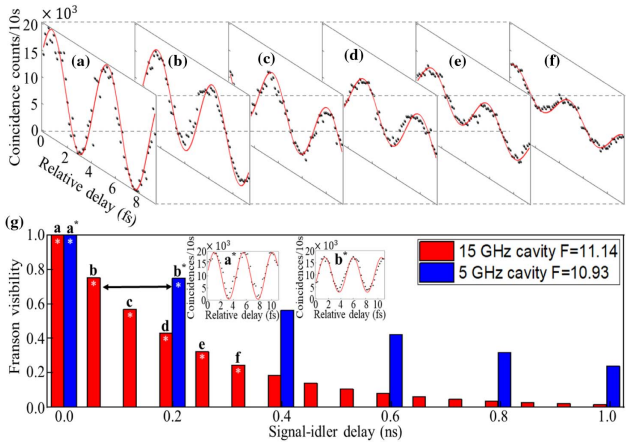

Fig. 2. Experimentally observed discretized time-energy entanglement using 5.03 GHz and 15.15 GHz FSR singly filtered BFCs. (a)–(f) Franson recurrence interference fringes with six discrete time bins measured in a 15.15 GHz FSR singly filtered BFC. (g) Theoretical Franson revival visibilities for 15.15 GHz and 5.03 GHz FSR singly filtered BFCs with superimposed experimental observations. Further included in a^* and b^* are measured Franson recurrence time bins in a 5.03 GHz FSR singly filtered BFC. The experimentally measured (theoretical) visibilities for the six time bins (in red) for the 15.15 GHz FSR singly filtered BFC are 98.97% (100%), 74.32% (75.43%), 54.37% (56.89%), 40.56% (42.91%), 31.5% (32.37%), and 22.32% (24.41%), respectively. For the two time bins in a 5.03 GHz FSR singly filtered BFC, the experimentally measured (theoretical) visibilities are 97.79% (100%) and 72.23% (75.03%), respectively. The two bidirectional black horizontal arrows indicate the similarity of Franson revival visibilities between two cavities. All measurements are performed with a coincidence window of 2 ns and the reported visibilities are after subtracting accidental coincidences.

Figure 3 presents the modeling and measurement of the normalized signal-idler temporal second-order cross-correlation function and Franson interference recurrence visibilities for the two cavities. To better resolve the mode-locked oscillations, we set the FWHM timing jitter to be 20 ps, relevant to current state-of-the-art low-jitter superconducting single-photon detectors [56]. In Figs. 3(a) and 3(b), we plot the signal-idler temporal second-order cross-correlation function of 5.03 GHz [experiment is presented in Fig. 1(b)] and 15.15 GHz FSR cavities with different cavity finesses F for comparison. Both results show that when the cavity finesse F increases to 30 in cavities under the same FSR, the cavity damping rate becomes smaller, resulting in an increased probability to detect signal photons at multiples of the cavity round-trip time t_{rt} after idler photons arrive at the single-photon detector. We observe a similar trend for Franson interference recurrence visibilities (measurements results are given in Fig. 2) as shown in Figs. 3(c) and 3(d). There is a clear improvement of modeled Franson visibilities when the cavity finesse F is ≈3 times larger than our experimental results in Fig. 2. For the 5.03 GHz FSR singly filtered BFC, we find that a small cavity finesse F of 30 can result in all the Franson interference recurrence visibilities to be higher than the quantum-classical limit of 70.7% [37,57] in the 1 ns temporal range. For the 15.15 GHz FSR singly

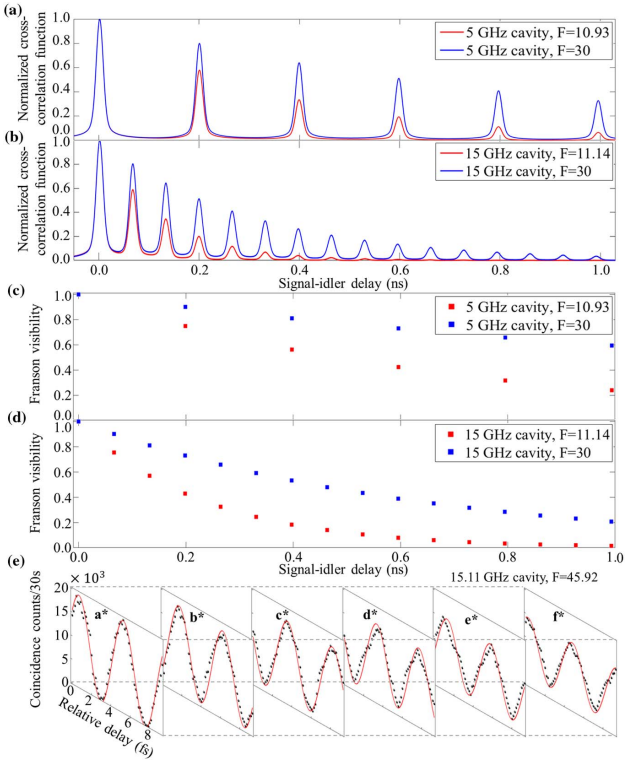

Fig. 3. Modeled and experimental mode-locking oscillations, Franson revival visibilities for 5.03 GHz, 15.15 GHz, and 15.11 GHz FSR singly filtered BFCs. (a) and (b) Theoretical signal-idler cross-correlation functions for the 5.03 GHz and 15.15 GHz FSR singly filtered BFCs with cavity finesse F of 10.93 [experiment data for cavity finesse F of 10.93 shown in the inset of Fig. 1(b)], 30, 11.14, and 30, respectively. For calculations in (a) and (b), the FWHM timing jitter of the single-photon detector is set at 20 ps. (c) and (d) Modeled Franson recurrence visibilities for the 5.03 GHz and 15.15 GHz FSR singly filtered BFCs with varied cavity finesses F of 10.93, 30, 11.14, and 30. Note that for 5.03 GHz FSR with a cavity finesses F of 10.93 GHz, and for 15.15 GHz FSR with a cavity finesse F of 11.14 singly filtered BFCs, our measurement results are provided in Fig. 2. Due to the increasing probability of detecting mode-locked temporal oscillations at the single-photon detector with a cavity finesse F of 30, the Franson interference recurrence visibilities increase correspondingly. This exemplifies that the cavity finesse F is a key parameter for optimizing the temporal correlations and Franson interference recurrence of the mode-locked biphoton states. (e) Experimentally measured Franson interference recurrence using a 15.11 GHz FSR, cavity finesse F 45.92 singly filtered BFC. a*–f* Franson recurrence interference fringes with six discrete time bins measured in a 45.92 cavity finesse F singly filtered BFC. The experimentally measured (theoretical) visibilities for the six time bins (in red) for the 15.11 GHz FSR singly filtered BFC are 98.76% (100%), 92.69% (93.39%), 86.45% (87.21%), 80.64% (81.45%), 75.01% (76.06%), and 69.86% (71.03%), respectively. All measurements are performed with a coincidence window of 2 ns and the reported visibilities are after subtracting accidental coincidences.

filtered BFC, the Franson visibility at the 16th time bin with cavity finesse F of 30 is ≈14-fold higher than that with cavity finesse F of 11.14. Due to the increasing probability of detecting mode-locked temporal oscillations at the single-photon detector with a cavity finesse F of 30, the Franson interference recurrence visibilities increase correspondingly. Here, via using a 45.92 cavity finesse F with a 15.11 GHz FSR singly filtered BFC, we experimentally demonstrate improved Franson interference recurrence. Figure 3(e) shows the Franson recurrence interference fringes with six discrete time bins measured in a 45.92 cavity finesse F singly filtered BFC. The experimentally measured (theoretical) visibilities for the six time bins (in red) for the 15.11 GHz FSR singly filtered BFC are 98.76% (100%), 92.69% (93.39%), 86.45% (87.21%), 80.64% (81.45%), 75.01% (76.06%), and 69.86% (71.03%), respectively. All measurements are performed with a coincidence window of 2 ns, and the reported visibilities are after subtracting accidental coincidences. This exemplifies that the cavity finesse F is a key parameter for optimizing both the temporal correlations and the Franson interference recurrence of the mode-locked biphoton states.

D. Discussions

Cavity finesse F tailors the intrinsic joint biphoton properties of mode-locked singly filtered BFCs as shown earlier in the Franson interference recurrence and signal-idler temporal second-order cross-correlation function. For the above signal-idler temporal second-order cross-correlation functions and Franson interference recurrence, cavity finesse F plays a key role because it is proportional to the number of round trips before a single photon leaves the cavity or is lost via dissipation. Indeed, from Eq. (2), for our linear planar FP cavity, the cavity finesse F is proportional to cavity quality factor Q. Therefore, increasing the cavity finesse F is equivalent to increasing the cavity Q factor where photons can travel more round trips in the cavity, whereas, storing more energy before they are lost in dissipation or leave the cavity. This results in a lower cavity damping rate with the same FSR, therefore, increasing the detection probability in signal-idler temporal second-order cross-correlation function after multiple cavity round-trip times t_{rt}. This flattens the time-energy entangled Franson recurrence interferences. In our case, the design of FP cavity mostly depends on our measurement setups. The FSR decides the frequency-bin spacing, time interval t_{rt}, and Franson revival periods, whereas, our motorized stage delay in arm2 of Franson interferometry sets the measurable Franson interference recurrence. Therefore, in order to access multiple time and frequency bins of our singly filtered BFCs, we choose to use 5 GHz and 15 GHz FSR cavities in this paper. In our prior works, we implemented a larger cavity FSR for denser Franson revival interferences, whereas, having less frequency bins in our BFC [3,4]. The bandwidth of the cavity, which is related to its finesse F and FSR, can be chosen to achieve higher detection rate in signal-idler temporal second-order cross-correlation function and to approach flattened Franson revival interferences.

In Fig. 4, we present the temporal second-order cross-correlation peak values and Franson interference recurrences for the 6th and 16th time bin in 15 GHz FSR singly filtered BFCs for higher cavity finesse F. For mode-locked oscillations in the temporal domain, we plot signal-idler temporal second-order cross-correlation peak values versus different cavity finesse F of 11.14, 30, 50, 100, and 200 in a 15.15 GHz FSR cavity with an FWHM timing jitter of 20 ps as shown in Fig. 4(a). It can be seen that by using a moderate cavity

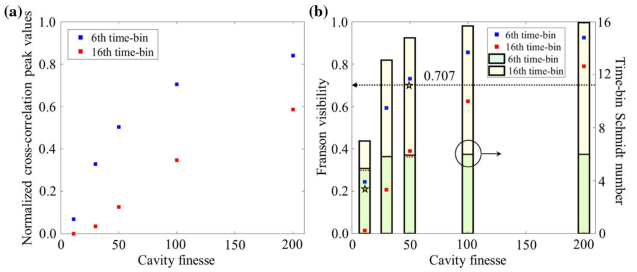

Fig. 4. Towards optimum mode-locked oscillations, Franson interference recurrence, and time-bin Schmidt number K_T in 15 GHz singly filtered BFCs. (a) Theoretical signal-idler cross-correlation peak values for 15.15 GHz FSR singly filtered BFCs with cavity finesse F of 11.14, 30, 50, 100, and 200, respectively. (b) Franson recurrence visibilities and time-bin Schmidt number K_T for 15.15 GHz FSR singly filtered BFC with cavity finesse F of 11.14, 30, 50, 100, and 200, respectively. The experimentally measured Franson visibilities (orange stars) are superimposed for a 15.15 GHz FSR cavity with a finesse F of 11.14, and a 15.11 GHz FSR cavity with a higher finesse F of 45.92, respectively. The measured sixth time-bin Franson visibility for a 15.11 GHz FSR cavity with a higher finesse F of 45.92 is 69.86% (71.03% for theoretical visibility) after subtracting accidental coincidences, which is close to the visibility of the quantum-classical limit of 70.7% (the black dotted line). Here, by using a higher cavity finesse F of 45.92, we observe an experimental ≈3.13-fold improvement of the Franson visibility compared to the Franson visibility with a cavity finesse F of 11.14 at the sixth time bin. Besides, for the 16th time bin in same BFC, there is a potential ≈24-fold improvement of the Franson visibility for a cavity finesse F of 45.92 compared to the Franson visibility with a cavity finesse F of 11.14. As cavity finesse F increases to 200 for the 16th time bin, the time-bin Schmidt number K_T becomes ≈16, which is because the Franson revival visibility approaches optimum limit of 100%. The light green and yellow bars represent the theoretical time-bin Schmidt number K_T from the Franson recurrence visibilities up to 6th and 16th time bins, respectively. The deep red dotted lines are the experimental time-bin Schmidt number K_T at the sixth time bin.

finesse F of 200 for both the 6th and the 16th time bins, signal photons are more likely to be detected after idler photons are counted at the detector, resulting in higher temporal correlation peak values. This improved JTI may be useful for temporal-multiplexing using singly filtered BFCs. In Fig. 4(b), we illustrate the effect of cavity finesse F on Franson interference recurrences and time-bin Schmidt number K_T with our experimental results of a cavity finesse F of 11.14 and a higher cavity finesse F of 45.92 superimposed (orange stars).

The improvement of Franson interference recurrence is described in Eq. (5). The measured sixth time-bin Franson visibility for a 15.11 GHz FSR cavity with a higher finesse F of 45.92 is 69.86% (71.03% for theoretical visibility) after subtracting accidental coincidences, which is very close to the visibility of quantum-classical limit of 70.7% (the black dotted line). Here, by using a cavity with higher finesse F of 45.92, we observe an experimental ≈3.13-fold improvement of the Franson visibility. All the other measurement data in 45.92 cavity finesse F singly filtered BFC are presented in Fig. 3(e). Besides, for the 16th time bin in the same BFC, there is a potential ≈24-fold improvement of the Franson visibility for a cavity finesse F of 45.92 compared to the Franson visibility with a cavity finesse F of 11.14. The light green and yellow bars represent the theoretical time-bin Schmidt number K_T from the Franson recurrence visibilities up to the 6th and 16th time bins, respectively. Here, we define time-bin Schmidt number K_T analog to the frequency-bin Schmidt number from literature [3,4,18,19]. In the time domain, we have a Schmidt number given by $K_T = (\sum \lambda_n^2)^{-1}$, where $\sum \lambda_n = 1$ with $\{\lambda_n\}$ being that domain's Schmidt mode eigenvalues. Then, due to the difficulty in measuring joint temporal amplitude (JTA), we use pure state assumption [3,4] such that JTA equals the square root of the binned JTI. By sampling the temporal wave function of our singly filtered BFC, at $\tau = n\Delta T_{\text{cavity}}$, we can obtain its binned JTI as $|\Psi(n\Delta T)|^2 = \frac{\exp(-2n\Delta\Omega\Delta T_{\text{cavity}})}{\sum_{n=0}^{N} \exp(-2n\Delta\Omega\Delta T_{\text{cavity}})}$. Combining the JTI of our singly filtered BFC and Eq. (5), we can obtain time-bin Schmidt mode eigenvalues as $\lambda_n = \frac{e^{-\pi n/F}}{\sum_{m=0}^{M} e^{-\pi m/F}}$, for $0 \le n \le M$, where $M+1$ is the number of Franson recurrence interference time bins. Therefore, given Franson recurrence interference visibility up to the 6th (experiment) and 16th (theory) time bins for 15 GHz singly filtered BFCs, we can extract their corresponding time-bin Schmidt number K_T. We note that this method can also be used for extracting the time-bin Schmidt number using Hong–Ou–Mandel revival interferences [2,3].

Deep red dotted lines are the experimentally measured sixth time-bin Schmidt number K_T of 4.82 (4.92 from theory) for a 11.14 cavity finesse F, and the sixth time-bin Schmidt number K_T of 5.91 (5.92 from theory) for a 45.92 cavity finesse F, respectively. As cavity finesse F increases to 200 for the 16th time bin, the time-bin Schmidt number K_T is equal to ≈16 effective modes, which is because the Franson revival visibility approaches the optimum limit of 100%. As illustrated in Fig. 4(b), we found out the time-bin Schmidt number K_T for a cavity finesse F of 200 is 15.92, and that for a cavity finesse F of 11.14 is 5.99. Hence, the effective temporal Hilbert space dimensionality, thus, potentially increases from 35 to 253. In Fig. 4, we choose to use cavities with FSR of 15 GHz because this FSR is closed to maximum FSR in cavity-enhanced SPDC sources [8,14,16,58–63]. Furthermore, this 15 GHz FSR cavity is compatible with the current fiber Bragg grating filters in optical communications for frequency-domain projection measurements [3]. Here, we note that our schemes are robust and flexible without requiring a stabilization system nor customized cavity design compared to cavity-enhanced SPDC sources [8,14,16,64–68]. Besides, in Fig. 8 of Appendix C, we also illustrate the effect of cavity finesse F on the temporal second-order cross-correlation function and Franson interference visibilities for a 50 GHz FSR singly filtered BFC. We note that the signal-idler temporal second-order cross-correlation function measurements are limited by the detection jitter of commercial single-photon detectors for 50 GHz FSR cavity, and they can be resolved by the Franson interference measurements experimentally accessible with current interferometric technology [2–5,69].

3. CONCLUSION

We have shown experimentally and theoretically that cavity finesse F acted on joint biphoton properties of mode-locked singly filtered BFCs, manifesting in the signal-idler temporal second-order cross-correlation function and Franson interference recurrence. We measured the similar trend of time-energy entanglement of 5.03 GHz and 15.15 GHz FSR mode-locked singly filtered BFCs via Franson interferometry with interference fringes observed over six and two time bins, and with optimum central time-bin accidental-subtracted visibility of 98.97% and 97.79%, respectively. Increasing the cavity finesse F from small to moderate values led to a lower cavity damping rate with the same FSR, increasing detection probability in the signal-idler temporal second-order cross-correlation function after multiple cavity round-trip times t_{rt} and flattening the visibility decay of the Franson interference recurrence in our singly filtered mode-locked BFCs. Via a higher cavity finesse F 45.92 singly filtered BFC, we experimentally present a ≈3.13-fold improvement of Franson visibility compared to the Franson visibility with cavity finesse F of 11.14 at the sixth time bin, close to the quantum-classical limit of 70.7%. Furthermore, for the 16th time bin in the same BFC, there was a potential ≈24-fold improvement of the Franson visibility for a cavity finesse F of 45.92 compared to the Franson visibility with a cavity finesse F of 11.14. By using a cavity finesse F of 200, we predicted a time-bin Schmidt number K_T near 16 effective modes, which was coming from the near-optimum Franson interference recurrence for all the time bins. Our results paved the way for optimum Franson interference recurrence towards scaling up the time-bin Schmidt number K_T and the Hilbert space dimensionality in the temporal domain, and for high-quality long-distance high-dimensional time-energy entanglement distribution and QKD.

APPENDIX A: DETAILS OF EXPERIMENTAL SETUP

In Fig. 5, we provide the details of the experimental scheme for generating singly filtered BFC. For our continuous-wave pumped source, we customize a tunable stabilized self-injection-locked 658 nm laser to achieve single-longitudinal mode lasing with wavelength tunability of several nanometers for optimizing the photon flux. We couple our tunable continuous-wave laser operating at ≈2 mW and ≈658 nm into a 1.6 cm long ppKTP waveguide, temperature controlled at 26.5°C for SPDC under type-II phase matching [2–5]. The fiber-coupled SPDC outputs are collimated in a low-loss fiber bench and sent through a long-pass filter (LPF) to block the pump, followed by a 1.3 nm BPF centered at 1316 nm to clean the SPDC spectrum further. We use an FPC and an FPBS to separate and balance the orthogonally polarized signal and idler photons, coupling them into their respective SMF-28 single-mode optical fibers. The three-fiber FP cavities are placed in the signal path for singly filtered BFCs generation. We carefully tune the fiber cavity temperature to align its transmission peaks with the generated entangled photons to maximize the coincidences of our singly filtered BFCs.

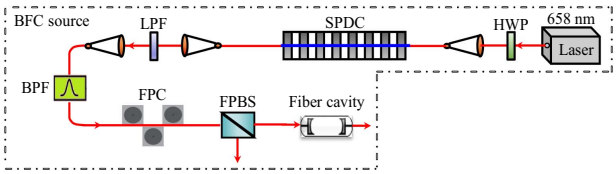

Fig. 5. Details of the experimental scheme for generating singly filtered BFCs. For our continuous-wave pumped source, we customize a tunable stabilized self-injection-locked 658 nm laser to achieve single-longitudinal mode lasing with wavelength tunability of several nanometers for optimizing the photon flux. We couple our tunable continuous-wave laser operating at ≈2 mW and ≈658 nm into a 1.6 cm long ppKTP waveguide, temperature controlled to 26.5°C for SPDC under type-II phase matching [2–5]. Then, three-fiber FP cavities are placed in the signal path for singly filtered BFCs generation. We carefully tune the fiber cavity temperature to align its transmission peaks with the generated entangled photons to maximize the coincidences of our singly filtered BFCs. LPF, long-pass filter; BPF, band-pass filter; FPC, fiber polarization controller; FPBS, fiber polarizing beam splitter.

APPENDIX B: MEASURED SIGNATURE OF FRANSON INTERFERENCES FOR 5.03 GHz AND 15.15 GHz FSR SINGLY FILTERED BFCS

In this section, we present the experimental measurements for the signature of Franson interference using our setup in main text Fig. 1(a). We measure three correlation peaks for different phase shifts induced by varying the thermal heater in the long path of arm1 of our Franson interferometry where it is clear that only the central peak intensity changes, whereas, the lateral peaks are unaffected. The phases for the measurements reported in Figs. 6(a) and 6(c) are such that the middle peak was maximized and minimized, respectively. By postselecting the central correlation peak and changing the phases of the interferometers (ΔT_1), we obtain a maximum Franson visibility for the 0th time bin over 98.99% in a 15.15 GHz FSR singly filtered BFC after subtracting accidental coincidences.

Then, in Figs. 7(a) and 7(b), we proceed to measure the noninteger cavity round-trip time Franson interferences for 5.03 GHz and 15.15 GHz FSR mode-locked singly filtered BFCs. When we translate the motorized stage with a ΔT_2 that is the noninteger cavity round-trip time, such as 360 ps, we observe an absence of the Franson interference fringes. The measured average coincidence counts are consistent with our results in the main text, Fig. 2. This confirms the Franson

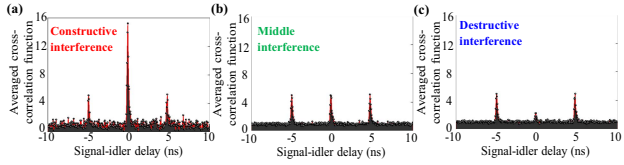

Fig. 6. Signature of Franson interference in the quantum regime. The phases for the measurements reported in (a) and (c) are such that the middle peak was maximized and minimized, respectively. By postselecting the central correlation peak and changing the phases of the interferometers (ΔT_1), we obtain a maximum Franson visibility for the 0th time bin over 98.99% in a 15.15 GHz FSR singly filtered BFC after subtracting accidental coincidences.

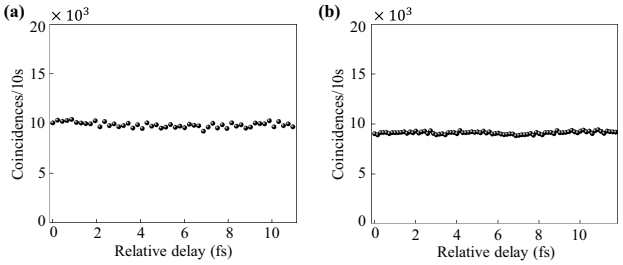

Fig. 7. Measured Franson interferences at noninteger cavity round-trip times in the 5.03 GHz and 15.15 GHz FSR mode-locked singly filtered BFCs. When we translate the motorized stage with a ΔT_2 that is noninteger cavity round-trip time, such as 360 ps, we observe an absence of the Franson interference fringes for 5.03 GHz FSR and 15.15 GHz FSR singly filtered BFCs in (a) and (b), respectively. This confirms the Franson interference recurrence only occurs when temporal delay is equal to integer of cavity round-trip times.

interference recurrence only occurs when temporal delay is equal to integer of cavity round-trip times.

APPENDIX C: MODELING OF TEMPORAL SECOND-ORDER CROSS-CORRELATION FUNCTION AND FRANSON RECURRENCE FOR A 50 GHz FSR SINGLY FILTERED MODE-LOCKED BFC

Finally, in this appendix, we provide the modeling of signal-idler temporal second-order cross-correlation function and Franson revivals visibility for a 50 GHz FSR cavity singly filtered mode-locked BFC. In Fig. 8(a), we model the signal-idler temporal second-order cross-correlation function versus four different cavity finesses F in a 50 GHz FSR cavity with an FWHM jitter of 20 ps. Due to the denser temporal spacing of mode-locked oscillations from a larger cavity FSR (compared to the 15.15 GHz FSR in the main text, for example) for a cavity finesse F of 500, there is a more than 50% probability to detect signal photons at 49 cavity round-trip times t_{rt} after idler photons are counted at detector across the whole 2 ns temporal range. In Fig. 8(b), we plot the Franson interference recurrences for four different cavity finesses F of 30, 100, 200, and 500 in the same temporal range. We note that with a moderate cavity finesse F of 500, all of the Franson interference recurrence visibilities surpass the quantum-classical threshold of 70.7% [37,57], confirming the time-energy entanglement over a 2 ns temporal range.

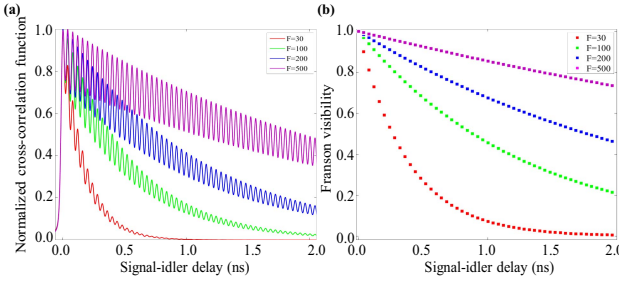

Fig. 8. Modeling of the signal-idler temporal second-order cross-correlation function and Franson revivals visibility for a 50 GHz FSR cavity singly filtered mode-locked BFC with different finesses F. In (a), we model the signal-idler temporal second-order cross-correlation function versus four different cavity finesses F in a 50 GHz FSR cavity with an FWHM timing jitter of 20 ps. In (b), we plot the Franson interference recurrences for four different cavity finesses F of 30, 100, 200, and 500 in the same temporal range.

Funding. U.S. Army Research Office Multidisciplinary Research Program of the University Research Initiative (MURI) (W911NF2120214); National Science Foundation (1741707 (EFRI ACQUIRE), 1919355, 1936375 (QII-TAQS)).

Acknowledgment. The authors acknowledge discussions with Z. Xie, P. Fan, J. H. Shapiro, F. N. C. Wong, and discussions on the superconducting single-photon detectors with V. Anant, B. Korzh, A. Mueller, M. Spiropulu, and M. Shaw. K.-C.C. and X.C. developed the idea, performed the measurements, and conducted data analysis. K.-C.C. and M.C.S. contributed to the theory and numerical modeling. K.-C.C., X.C., and C.W.W. prepared the paper. All authors contributed to the discussion and revision of the paper.

Disclosures. The authors declare no conflicts of interest.

Data Availability. All data needed to evaluate the conclusions in the paper are present in the paper. Additional data related to this paper may be requested from the authors.

REFERENCES

1. Y. J. Lu, R. L. Campbell, and Z. Y. Ou, "Mode-locked two-photon states," Phys. Rev. Lett. **91**, 163602 (2003).
2. Z. Xie, T. Zhong, S. Shrestha, X. Xu, J. Liang, Y.-X. Gong, J. C. Bienfang, A. Restelli, J. H. Shapiro, F. N. C. Wong, and C. W. Wong, "Harnessing high-dimensional hyperentanglement through a biphoton frequency comb," Nat. Photonics **9**, 536–542 (2015).
3. K.-C. Chang, X. Cheng, M. C. Sarihan, A. K. Vinoid, Y. S. Lee, T. Zhong, Y.-X. Gong, Z. Xie, J. H. Shapiro, F. N. C. Wong, and C. W. Wong, "648 Hilbert space dimensionality in a biphoton frequency comb: entanglement of formation and Schmidt mode decomposition," npj Quantum Inf. **7**, 48 (2021).
4. K.-C. Chang, X. Cheng, M. C. Sarihan, F. N. C. Wong, J. H. Shapiro, and C. W. Wong, "High-dimensional energy-time entanglement distribution via a biphoton frequency comb," in *Conference on Lasers and Electro-Optics*, OSA Technical Digest (Optical Society of America, 2021), paper FF1A.7.
5. K.-C. Chang, X. Cheng, M. C. Sarihan, W. Wang, F. N. C. Wong, J. H. Shapiro, and C. W. Wong, "Mode-locked phase coherent singly-resonant biphoton frequency comb," in *Conference on Lasers and Electro-Optics*, OSA Technical Digest (Optical Society of America, 2022), paper FTh5O.4.70.
6. J. H. Shapiro, "Coincidence dips and revivals from a Type-II optical parametric amplifier," in *Conference on Nonlinear Optics* (Optical Society of America, 2002), paper FC7-1.
7. C. E. Kuklewicz, F. N. C. Wong, and J. H. Shapiro, "Time-bin-modulated biphotons from cavity-enhanced down-conversion," Phys. Rev. Lett. **97**, 223601 (2006).
8. M. Scholz, F. Wolfgramm, U. Herzog, and O. Benson, "Narrow-band single photons from a single-resonant optical parametric oscillator far below threshold," Appl. Phys. Lett. **91**, 191104 (2007).
9. M. Scholz, L. Koch, and O. Benson, "Statistics of narrow-band single photons for quantum memories generated by ultrabright cavity-enhanced parametric down-conversion," Phys. Rev. Lett. **102**, 063603 (2009).

10. F. Wolfgramm, Y. A. de Icaza Astiz, F. A. Beduini, A. Ceré, and M. W. Mitchell, "Atom-resonant heralded single photons by interaction-free measurement," Phys. Rev. Lett. **106**, 053602 (2011).
11. D. Rieländer, K. Kutluer, P. M. Ledingham, M. Gündoğan, J. Fekete, M. Mazzera, and H. De Riedmatten, "Quantum storage of heralded single photons in a praseodymium-doped crystal," Phys. Rev. Lett. **112**, 040504 (2014).
12. A. Seri, A. Lenhard, D. Rieländer, M. Gündoğan, P. M. Ledingham, M. Mazzera, and H. De Riedmatten, "Quantum correlations between single telecom photons and a multimode on-demand solid-state quantum memory," Phys. Rev. X **7**, 021028 (2017).
13. A. Seri, D. Lago-Rivera, A. Lenhard, G. Corrielli, R. Osellame, M. Mazzera, and H. de Riedmatten, "Quantum storage of frequency-multiplexed heralded single photons," Phys. Rev. Lett. **123**, 080502 (2019).
14. R. Ikuta, R. Tani, M. Ishizaki, S. Miki, M. Yabuno, H. Terai, N. Imoto, and T. Yamamoto, "Frequency-multiplexed photon pairs over 1000 modes from a quadratic nonlinear optical waveguide resonator with a singly resonant configuration," Phys. Rev. Lett. **123**, 193603 (2019).
15. D. Lago-Rivera, S. Grandi, J. V. Rakonjac, A. Seri, and H. de Riedmatten, "Telecom-heralded entanglement between multimode solid-state quantum memories," Nature **594**, 37–40 (2021).
16. T. Yamazaki, R. Ikuta, T. Kobayashi, S. Miki, F. China, H. Terai, N. Imoto, and T. Yamamoto, "Massive-mode polarization entangled biphoton frequency comb," Sci. Rep. **12**, 8964 (2022).
17. C. Reimer, M. Kues, P. Roztocki, B. Wetzel, F. Grazioso, B. E. Little, S. T. Chu, T. Johnston, Y. Bromberg, L. Caspani, D. J. Moss, and R. Morandotti, "Generation of multiphoton entangled quantum states by means of integrated frequency combs," Science **351**, 1176–1180 (2016).
18. J. A. Jaramillo-Villegas, P. Imany, O. D. Odele, D. E. Leaird, Z.-Y. Ou, M. Qi, and A. M. Weiner, "Persistent energy-time entanglement covering multiple resonances of an on-chip biphoton frequency comb," Optica **4**, 655–663 (2017).
19. M. Kues, C. Reimer, P. Roztocki, L. Romero Cortés, S. Sciara, B. Wetzel, Y. Zhang, A. Cino, S. T. Chu, B. E. Little, D. J. Moss, L. Caspani, J. Azaña, and R. Morandotti, "On-chip generation of high-dimensional entangled quantum states and their coherent control," Nature **546**, 622–626 (2017).
20. H.-H. Lu, J. M. Lukens, N. A. Peters, B. P. Williams, A. M. Weiner, and P. Lougovski, "Quantum interference and correlation control of frequency-bin qubits," Optica **5**, 1455 (2018).
21. P. Imany, N. B. Lingaraju, M. S. Alshaykh, D. E. Leaird, and A. M. Weiner, "Probing quantum walks through coherent control of high-dimensionally entangled photons," Sci. Adv. **6**, eaba8066 (2020).
22. R. H. Brown and R. Q. Twiss, "A test of a new type of stellar interferometer on Sirius,"; Nature **178**, 1046–1048 (1956).
23. N. B. Lingaraju, H.-H. Lu, S. Seshadri, P. Imany, D. E. Leaird, J. M. Lukens, and A. M. Weiner, "Quantum frequency combs and Hong-Ou-Mandel interferometry: the role of spectral phase coherence," Opt. Express **27**, 38683–38697 (2019).
24. J. Wang, S. Paesani, Y. Ding, R. Santagati, P. Skrzypczyk, A. Salavrakos, J. Tura, R. Augusiak, L. Mančinska, D. Bacco, D. Bonneau, J. W. Silverstone, Q. Gong, A. Acín, K. Rottwitt, L. K. Oxenløøwe, J. L. O'Brien, A. Laing, and M. G. Thompson, "Multidimensional quantum entanglement with large-scale integrated optics," Science **360**, 285–291 (2018).
25. C. Reimer, S. Sciara, P. Roztocki, M. Islam, L. R. Cortés, Y. Zhang, B. Fischer, S. Loranger, R. Kashyap, A. Cino, S. T. Chu, B. E. Little, D. J. Moss, L. Caspani, W. J. Munro, J. Azaña, M. Kues, and R. Morandotti, "High-dimensional one-way quantum processing implemented on *d*-level cluster states," Nat. Phys. **15**, 148–153 (2018).
26. D. Llewellyn, Y. Ding, I. I. Faruque, S. Paesani, D. Bacco, R. Santagati, Y.-J. Qian, Y. Li, Y.-F. Xiao, M. Huber, M. Malik, G. F. Sinclair, X. Zhou, K. Rottwitt, J. L. O'Brien, J. G. Rarity, Q. Gong, L. K. Oxenlowe, J. Wang, and M. G. Thompson, "Chip-to-chip quantum teleportation and multi-photon entanglement in silicon," Nat. Phys. **16**, 148–153 (2020).
27. J. Wang, F. Sciarrino, A. Laing, and M. G. Thompson, "Integrated photonic quantum technologies," Nat. Photonics **14**, 273–284 (2020).
28. I. Ali Khan, C. J. Broadbent, and J. C. Howell, "Large-alphabet quantum key distribution using energy-time entangled bipartite states," Phys. Rev. Lett. **98**, 060503 (2007).
29. T. Zhong, H. Zhou, R. D. Horansky, C. Lee, V. B. Verma, A. E. Lita, A. Restelli, J. C. Bienfang, R. P. Mirin, T. Gerrits, S. W. Nam, F. Marsili, M. D. Shaw, Z. Zhang, L. Wang, D. Englund, G. W. Wornell, J. H. Shapiro, and F. N. C. Wong, "Photon-efficient quantum key distribution using time-energy entanglement with high-dimensional encoding," New J. Phys. **17**, 022002 (2015).
30. N. T. Islam, C. C. W. Lim, C. Cahall, J. Kim, and D. J. Gauthier, "Provably secure and high-rate quantum key distribution with time-bin qudits," Sci. Adv. **3**, e1701491 (2017).
31. C. Lee, D. Bunandar, Z. Zhang, G. R. Steinbrecher, P. B. Dixon, F. N. C. Wong, J. H. Shapiro, S. A. Hamilton, and D. Englund, "Large-alphabet encoding for higher-rate quantum key distribution," Opt. Express **27**, 17539–17549 (2019).
32. I. Vagniluca, B. Da Lio, D. Rusca, D. Cozzolino, Y. Ding, H. Zbinden, A. Zavatta, L. K. Oxenløwe, and D. Bacco, "Efficient time-bin encoding for practical high-dimensional quantum key distribution," Phys. Rev. Appl. **14**, 014051 (2020).
33. V. Tamma and S. Laibacher, "Multiboson correlation interferometry with arbitrary single-photon pure states," Phys. Rev. Lett. **114**, 243601 (2015).
34. X.-J. Wang, B. Jing, P.-F. Sun, C.-W. Yang, Y. Yu, V. Tamma, X.-H. Bao, and J.-W. Pan, "Experimental time-resolved interference with multiple photons of different colors," Phys. Rev. Lett. **121**, 080501 (2018).
35. S. Laibacher and V. Tamma, "From the physics to the computational complexity of multiboson correlation interference," Phys. Rev. Lett. **115**, 243605 (2015).
36. A. P. Lund, M. J. Bremner, and T. C. Ralph, "Quantum sampling problems, BosonSampling and quantum supremacy," npj Quantum Inf. **3**, 15 (2017).
37. J. D. Franson, "Bell inequality for position and time," Phys. Rev. Lett. **62**, 2205–2208 (1989).
38. F. Vedovato, C. Agnesi, M. Tomasin, M. Avesani, J.-Å. Larsson, G. Vallone, and P. Villoresi, "Postselection-loophole-free Bell violation with genuine time-bin entanglement," Phys. Rev. Lett. **121**, 190401 (2018).
39. I. Marcikic, H. de Riedmatten, W. Tittel, H. Zbinden, M. Legré, and N. Gisin, "Distribution of time-bin entangled qubits over 50 km of optical fiber," Phys. Rev. Lett. **93**, 180502 (2004).
40. T. Honjo, H. Takesue, H. Kamada, Y. Nishida, O. Tadanaga, M. Asobe, and K. Inoue, "Long-distance distribution of time-bin entangled photon pairs over 100 km using frequency up-conversion detectors," Opt. Express **15**, 13957–13964 (2007).
41. J. F. Dynes, H. Takesue, Z. L. Yuan, A. W. Sharpe, K. Harada, T. Honjo, H. Kamada, O. Tadanaga, Y. Nishida, M. Asobe, and A. J. Shields, "Efficient entanglement distribution over 200 kilometers," Opt. Express **17**, 11440–11449 (2009).
42. T. Inagaki, N. Matsuda, O. Tadanaga, M. Asobe, and H. Takesue, "Entanglement distribution over 300 km of fiber," Opt. Express **21**, 23241–23249 (2013).
43. D. Aktas, B. Fedrici, F. Kaiser, T. Lunghi, L. Labonté, and S. Tanzilli, "Entanglement distribution over 150 km in wavelength division multiplexed channels for quantum cryptography," Laser Photon. Rev. **10**, 451–457 (2016).
44. K. Niizeki, D. Yoshida, K. Ito, I. Nakamura, N. Takei, K. Okamura, M.-Y. Zheng, X.-P. Xie, and T. Horikiri, "Two-photon comb with wavelength conversion and 20-km distribution for quantum communication," Commun. Phys. **3**, 138 (2020).
45. Z. Zhang, J. Mower, D. Englund, F. N. C. Wong, and J. H. Shapiro, "Unconditional security of time-energy entanglement quantum key distribution using dual-basis interferometry," Phys. Rev. Lett. **112**, 120506 (2014).
46. F. Xu, X. Ma, Q. Zhang, H.-K. Lo, and J.-W. Pan, "Secure quantum key distribution with realistic devices," Rev. Mod. Phys. **92**, 025002 (2020).
47. N. Sangouard, C. Simon, H. de Riedmatten, and N. Gisin, "Quantum repeaters based on atomic ensembles and linear optics," Rev. Mod. Phys. **83**, 33–80 (2011).

48. E. Saglamyurek, N. Sinclair, J. Jin, J. A. Slater, D. Oblak, F. Bussiéres, M. George, R. Ricken, W. Sohler, and W. Tittel, "Broadband waveguide quantum memory for entangled photons," Nature **469**, 512–515 (2011).
49. C. Clausen, I. Usmani, F. Bussiéres, N. Sangouard, M. Afzelius, H. de Riedmatten, and N. Gisin, "Quantum storage of photonic entanglement in a crystal," Nature **469**, 508–511 (2011).
50. E. Saglamyurek, J. Jin, V. B. Verma, M. D. Shaw, F. Marsili, S. W. Nam, D. Oblak, and W. Tittel, "Quantum storage of entangled telecom-wavelength photons in an erbium-doped optical fibre," Nat. Photonics **9**, 83–87 (2015).
51. E. Saglamyurek, M. G. Puigibert, Q. Zhou, L. Giner, F. Marsili, V. B. Verma, S. W. Nam, L. Oesterling, D. Nippa, D. Oblak, and W. Tittel, "A multiplexed light-matter interface for fibre-based quantum networks," Nat. Commun. **7**, 11202 (2016).
52. A. Tiranov, P. C. Strassmann, J. Lavoie, N. Brunner, M. Huber, V. B. Verma, S. W. Nam, R. P. Mirin, A. E. Lita, F. Marsili, M. Afzelius, F. Bussières, and N. Gisin, "Temporal multimode storage of entangled photon pairs," Phys. Rev. Lett. **117**, 240506 (2016).
53. F. Steinlechner, S. Ecker, M. Fink, B. Liu, J. Bavaresco, M. Huber, T. Scheidl, and R. Ursin, "Distribution of high-dimensional entanglement via an intra-city free-space link," Nat. Commun. **8**, 15971 (2017).
54. T. Ikuta and H. Takesue, "Four-dimensional entanglement distribution over 100 km," Sci. Rep. **8**, 7 (2018).
55. T. Zhong, F. N. C. Wong, T. D. Roberts, and P. Battle, "High performance photon-pair source based on a fiber-coupled periodically poled KTiOPO4 waveguide," Opt. Express **17**, 12019–12030 (2009).
56. B. A. Korzh, Q.-Y. Zhao, J. P. Allmaras, S. Frasca, T. M. Autry, E. A. Bersin, A. D. Beyer, R. M. Briggs, B. Bumble, M. Colangelo, G. M. Crouch, A. E. Dane, T. Gerrits, A. E. Lita, F. Marsili, G. Moody, C. Peña, E. Ramirez, J. D. Rezac, N. Sinclair, M. J. Stevens, A. E. Velasco, V. B. Verma, E. E. Wollman, S. Xie, D. Zhu, P. D. Hale, M. Spiropulu, K. L. Silverman, R. P. Mirin, S. W. Nam, A. G. Kozorezov, M. D. Shaw, and K. K. Berggren, "Demonstration of sub-3 ps temporal resolution with a superconducting nanowire single-photon detector," Nat. Photonics **14**, 250–255 (2020).
57. J. G. Rarity and P. R. Tapster, "Experimental violation of Bell's inequality based on phase and momentum," Phys. Rev. Lett. **64**, 2495–2498 (1990).
58. Z. Y. Ou and Y. J. Lu, "Cavity enhanced spontaneous parametric down-conversion for the prolongation of correlation time between conjugate photons," Phys. Rev. Lett. **83**, 2556–2559 (1999).
59. C. E. Kuklewicz, E. Keskiner, F. N. C. Wong, and J. H. Shapiro, "A high-flux entanglement source based on a doubly resonant optical parametric amplifier," J. Opt. B Quantum Semiclass. Opt. **4**, S162 (2002).
60. A. Lenhard, M. Bock, C. Becher, S. Kucera, J. Brito, P. Eich, P. Müller, and J. Eschner, "Telecom-heralded single-photon absorption by a single atom," Phys. Rev. A **92**, 063827 (2015).
61. O. Slattery, L. Ma, P. Kuo, and X. Tang, "Narrow-linewidth source of greatly non-degenerate photon pairs for quantum repeaters from a short singly resonant cavity," Appl. Phys. B **121**, 413–419 (2015).
62. M. Rambach, A. Nikolova, T. J. Weinhold, and A. G. White, "Sub-megahertz linewidth single photon source," APL Photon. **1**, 096101 (2016).
63. O. T. Slattery, L. Ma, K. Zong, and X. Tang, "Background and review of cavity-enhanced spontaneous parametric down-conversion," J. Res. Natl. Inst. Stan. Technol. **124**, 124019 (2019).
64. E. Pomarico, B. Sanguinetti, N. Gisin, R. Thew, H. Zbinden, G. Schreiber, A. Thomas, and W. Sohler, "Waveguide-based OPO source of entangled photon pairs," New J. Phys. **11**, 113042 (2009).
65. C.-S. Chuu, G. Y. Yin, and S. E. Harris, "A miniature ultrabright source of temporally long, narrowband biphotons," Appl. Phys. Lett. **101**, 051108 (2012).
66. J. Fekete, D. Rieländer, M. Cristiani, and H. de Riedmatten, "Ultranarrow-band photon-pair source compatible with solid state quantum memories and telecommunication networks," Phys. Rev. Lett. **110**, 220502 (2013).
67. A. Ahlrichs and O. Benson, "Bright source of indistinguishable photons based on cavity-enhanced parametric down-conversion utilizing the cluster effect," Appl. Phys. Lett. **108**, 021111 (2016).
68. P.-J. Tsai and Y.-C. Chen, "Ultrabright, narrow-band photon-pair source for atomic quantum memories," Quantum Sci. Technol. **3**, 034005 (2018).
69. A. Martin, T. Guerreiro, A. Tiranov, S. Designolle, F. Fröwis, N. Brunner, M. Huber, and N. Gisin, "Quantifying photonic high-dimensional entanglement," Phys. Rev. Lett. **118**, 110501 (2017).